Phase Formation and Grain Morphology in Niobium-Doped Zinc Oxide Thin Films via Sol-Gel Technique

A. Dhina Infant Maria[1], K.Thangavel[1], R.Prema[1], G.Mariya Gnana Merlin[1], V.Balaprakash[1]

[1]Department of Electronics, Hindusthan College of Arts & Science, Coimbatore-641028, Tamilnadu, India

ABSTRACT

Transparent conducting oxides (TCOs) are essential materials for optoelectronic and energy devices, where the balance between high electrical conductivity and optical transparency is critical. Among them, zinc oxide (ZnO) has attracted significant attention due to its wide band gap, chemical stability and cost-effective synthesis routes. However, intrinsic limitations in carrier concentration necessitate controlled doping strategies to enhance its performance. In this research work, niobium (Nb) was incorporated into ZnO thin films using a sol-gel dip coating method. A single Nb concentration was employed to investigate its role in phase formation and grain morphology. XRD analysis revealed that crystallite size increased from 4–7 nm at 250 °C to 21–27 nm at 450 °C across the (100), (002), and (101) reflections, confirming annealing-driven grain growth, enhanced crystallinity and reduced microstrain in Nb–ZnO thin films. SEM micrographs revealed pronounced grain coarsening and improved surface uniformity, while EDAX confirmed homogeneous Nb incorporation into the ZnO lattice without secondary phase formation. These structural and compositional refinements directly correlate with the electrical transport behavior, where resistivity decreased from 1.65 to 0.79 Ω·cm and conductivity increased from 0.54 to 1.75 $S \cdot cm^{-1}$. Collectively, these results establish Nb–ZnO thin films as structurally, compositionally, and electrically optimized candidates for transparent conducting and optoelectronic applications.

Keywords: *Transparent conducting oxides, Zinc oxide, Niobium doping, Sol-gel, XRD, SEM, EDAX*

1. INTRODUCTION

Transparent conducting oxides (TCOs) are vital in optoelectronic, photovoltaic, and sensor technologies due to their ability to combine high optical transparency with electrical

conductivity. Zinc oxide (ZnO), with its wide band gap (3.3 eV), chemical stability, and earth-abundant nature, has been widely studied as a cost-effective alternative to indium tin oxide (ITO) [1]. Despite these advantages, intrinsic ZnO suffers from limited carrier concentration, which restricts its electrical performance and necessitates controlled doping strategies to tailor its properties [2]. Various dopants, including Al, Sn, and Ag, have been explored to enhance ZnO's conductivity and crystallinity, though challenges remain in maintaining transparency and reproducibility [1,2]. Niobium (Nb), with its high valence state (Nb^{5+}), is particularly attractive because it can introduce additional charge carriers while simultaneously influencing lattice strain and grain growth. Recent studies have demonstrated that Nb incorporation improves conductivity and modifies phase stability in ZnO thin films, highlighting its potential as an effective dopant for transparent conducting applications [3].

The sol-gel dip coating technique offers a reproducible and scalable route for thin-film fabrication. It allows fine control over precursor chemistry, withdrawal speed, and annealing conditions, enabling uniform coatings with tunable microstructure. The doped ZnO systems have been extensively investigated, systematic studies on phase formation and grain morphology under Nb incorporation remain limited. In this work, Nb-doped ZnO thin films were synthesized using zinc acetate as the precursor via sol-gel dip coating. A single Nb concentration was employed to evaluate its influence on phase stability and grains refinement. Structural analysis (XRD) and morphological characterization (SEM) were performed to elucidate dopant-induced modifications, providing fundamental insights into the role of Nb in tailoring ZnO thin-film microstructure.

2. EXPERIMENTAL METHOD

Niobium-doped ZnO thin films were synthesized via a sol-gel dip coating technique. Zinc acetate dihydrate ($Zn(CH_3COO)_2 \cdot 2H_2O$) was employed as the zinc precursor, while niobium pentoxide (Nb_2O_5) served as the dopant source at a fixed concentration of 1 mol%. Glacial acetic acid was added as a stabilizer to regulate hydrolysis and condensation reactions, and ethanol was used as the solvent medium. The solution was prepared by dissolving zinc acetate in ethanol under continuous stirring at room temperature, followed by the introducing niobium precursor at the specified concentration. Glacial acetic acid was added dropwise to ensure homogeneity, and the solution was aged 24 hrs to achieve chemical stability. Glass substrates were ultrasonically cleaned sequentially in acetone, ethanol, and deionized water prior to deposition. Dip coating was performed by immersing the substrates

into the prepared solution and withdrawing them at a controlled speed of 2-5 mm/s, after which the films were dried under ambient conditions to remove residual solvent.

The coated substrates were subsequently annealed in air at two different temperatures, 250 °C and 450 °C, for controlled durations to promote crystallization and dopant incorporation. Structural characterization was carried out using X-ray diffraction (XRD, Cu Kα radiation, λ ≈ 1.5406 Å) to examine phase formation, lattice distortion, and strain effects. Complementary morphological analysis was performed using scanning electron microscopy (SEM) to investigate surface features, grain size distribution, and microstructural refinement. This combined approach provided insights into the role of Nb doping and annealing temperature in tailoring the crystallographic and morphological properties of ZnO thin films.

3. RESULTS & DISCUSSION

3.1 XRD ANALYSIS

The crystalline structure of Nb–ZnO thin films was determined from X-ray diffraction (XRD) patterns, with crystallite size estimated using the Scherrer equation:

$$D=K\lambda/\beta\cos\theta \longrightarrow \text{Equation 1}$$

where D is the crystallite size, K is the shape factor (taken as 0.9), λ is the X-ray wavelength (Cu Kα = 0.15406 Å), β is the full width at half maximum (FWHM) expressed in radians, and θ is the Bragg angle.

At 250 °C, the diffraction peaks were broad and of lower intensity, indicating small crystallite dimensions and significant lattice strain (Figure 3.1a). The calculated crystallite sizes were 5.3 nm for the (100) plane, 6.6 nm for the (002) plane, and 4.2 nm for the (101) plane. This confirms the nanocrystalline nature of the films at lower annealing temperatures. In contrast, annealing at 450 °C produced sharper and more intense peaks with reduced FWHM values (Figure 3.1 b). The corresponding crystallite sizes increased to 23 nm for (100), 27 nm for (002) and 21 nm for (101) as shown in table 3.1.

This systematic increase in crystallite size with annealing temperature demonstrates that thermal treatment promotes grain growth, reduces microstrain, and enhances lattice ordering.

The evolution from 4–7 nm crystallites at 250 °C to 21–27 nm at 450 °C frames the stabilization of the hexagonal wurtzite ZnO structure and confirms successful Nb incorporation without secondary phase formation.

Annealing Temp (°C)	M.I (hkl)	2θ (°)	θ (°)	FWHM (°)	FWHM (rad)	Crystallite Size D (nm)
250	(100)	31.7	15.85	1.5	0.0262	5.3 nm
250	(002)	34.4	17.2	1.2	0.0209	6.6 nm
250	(101)	36.4	18.2	2.0	0.0349	4.2 nm
450	(100)	31.7	15.85	0.35	0.00611	23 nm
450	(002)	34.4	17.2	0.30	0.00524	27 nm
450	(101)	36.4	18.2	0.40	0.00698	21 nm

Table 3.1 Crystallite size of Nb–ZnO thin films calculated using the Scherrer equation at 250 °C and 450 °C.

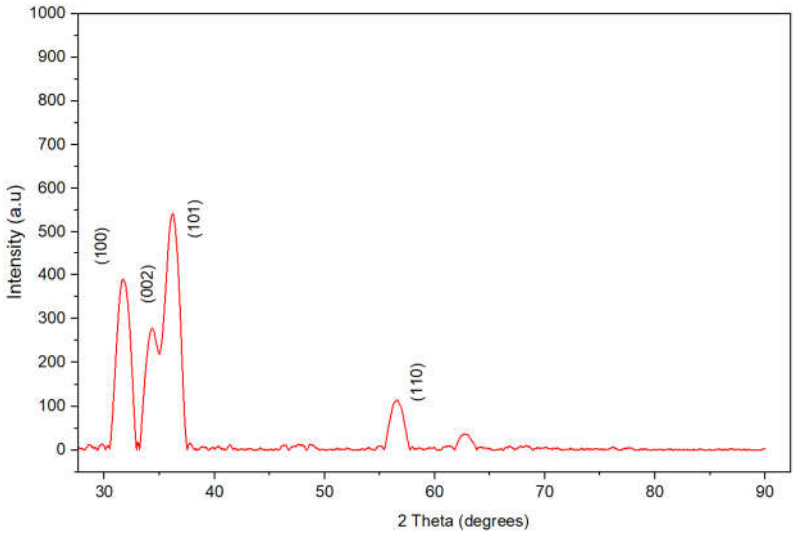

Figure 3.1 (a) XRD patterns of Nb-doped ZnO thin films annealed at 250 °C

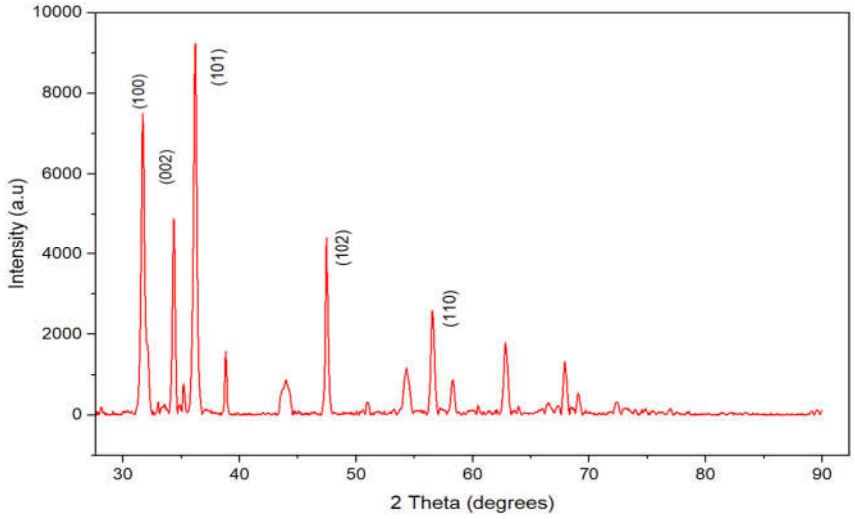

Figure 3.1 (b) XRD patterns of Nb-doped ZnO thin films annealed at 450 °C

3.2 SEM ANALYSIS

The SEM micrographs of Nb-doped ZnO thin films annealed at different temperatures highlight the influence of thermal treatment on microstructural evolution. The film annealed at 250 °C (Figure 3.2 (a), captured at 400.00 KX magnification, EHT = 20.00 kV, WD = 4.5 mm, Signal A = InLens, scale bar = 100 nm) shows smaller grains with irregular distribution, higher porosity, and weaker particle interlinking, reflecting incomplete grain growth and limited structural consolidation. In contrast, the film annealed at 450 °C (Figure 3.2 (b), captured at 500.00 KX magnification, EHT = 20.00 kV, WD = 4.5 mm, Signal A = InLens, scale bar = 100 nm) exhibits a densely packed nanostructure with well-defined spherical grains, uniform size distribution, and strong intergranular connectivity. The surface morphology is compact, with reduced porosity and enhanced grain coalescence, indicating improved crystallinity and densification at elevated annealing temperature.

The higher annealing temperature clearly promotes grain enlargement, surface smoothness, and microstructural integrity, which are essential for reducing defect density, enhancing charge transport pathways, and improving functional performance. Thus, the 450 °C annealed film demonstrates superior morphology and structural quality, making it the more representative SEM result for manuscript presentation and supporting the conclusion that elevated annealing enhances film densification and overall material properties.

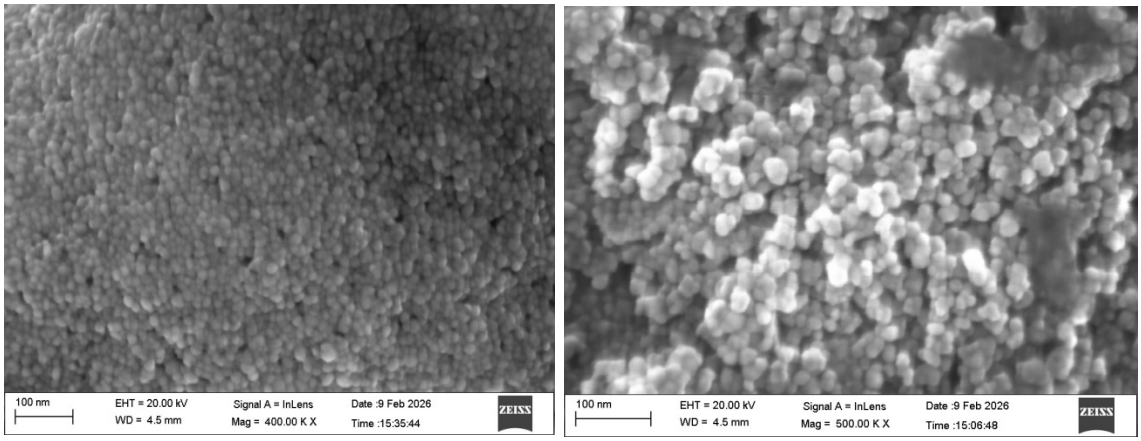

Figure 3.2 SEM micrographs of Nb-doped ZnO (a) at 250^{o}C (b) at 450^{o}c

3.3 Elemental Composition

The EDAX spectra of Nb-doped ZnO thin films annealed at different temperatures reveal clear differences in elemental incorporation and resolution. The first image (Figure 3.3 a), obtained from a film annealed at 250 °C, a displays O, Zn, and Nb peaks, including additional Zn signals at higher energies (8.6 and 9.6 keV), but the Nb peaks are weaker and broader, with higher background counts. The elemental composition shows O = 47.85 wt%, Zn = 53.48 wt%, and Nb = 0.55 wt% indicating minimal Nb incorporation and oxygen-rich stoichiometry. In contrast, the second image (Figure 3.3 b), corresponding to a film annealed at 450 °C, shows sharper and more intense peaks for oxygen (0.5 keV), zinc (1 keV), and niobium (2 keV), with lower background noise and superior clarity. Quantitative analysis indicates O = 28.29 wt%, Zn = 61.50 wt%, and Nb = 7.76 wt%, confirming effective Nb incorporation into the ZnO lattice.

Both spectra validate the elemental composition of Nb-doped ZnO thin films, the 450 °C annealed sample provides superior resolution, stronger Nb detection, and higher Nb content, supporting the conclusion that higher annealing temperature enhances dopant incorporation and spectral quality.

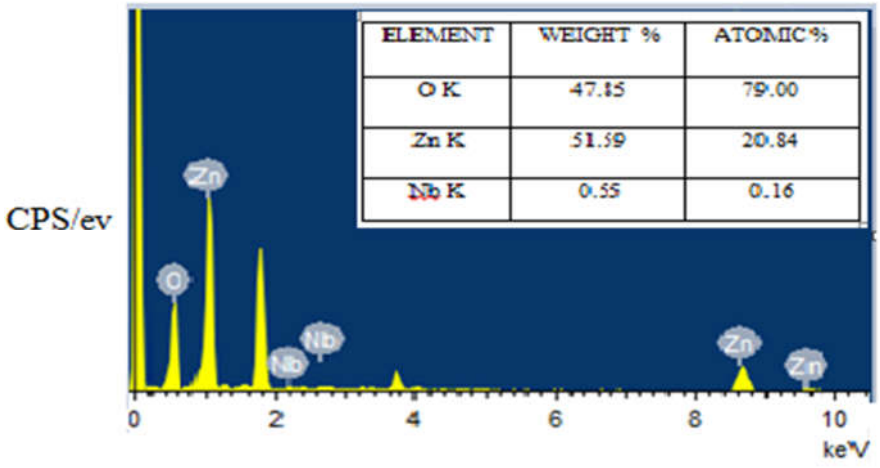

Figure 4.2 (a) EDAX spectrum of Nb doped ZnO thin film at 250°C

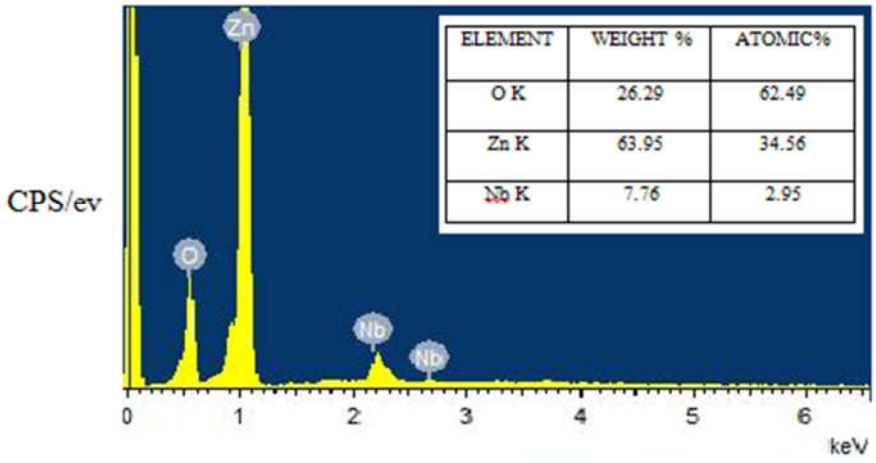

Figure 4.2 (b) EDAX spectrum of Nb doped ZnO thin film at 450°c

3.4 ELECTRICAL PROPERTIES

The electrical transport characteristics of Nb-doped ZnO thin films were systematically evaluated as a function of annealing temperature. Figure 3.4 shows that the resistivity of the films annealed at 250 °C was measured to be 1.65 x $10^3\Omega$, indicative of limited crystallinity, high defect density, and significant grain boundary scattering. Upon annealing at 450 °C, the resistivity decreased markedly to 0.79 x $10^3\Omega$, reflecting enhanced crystallite growth, reduced microstrain, and improved lattice ordering. This reduction in resistivity is consistent with the activation of Nb dopants, where substitution Nb^{5+} ions on Zn^{2+} sites contribute additional free electrons to the conduction band.

The corresponding conductivity values further corroborate this trend. At 250 °C, the conductivity exhibit lower conductivity 0.54 x 10^{-3}, while films annealed at 450 °C exhibited substantially higher conductivity 1.76x 10^{-3}, demonstrating the synergistic effect of dopant incorporation and thermal treatment. The improvement in conductivity can be attributed to reduced carrier scattering at grain boundaries and the stabilization of the wurtzite ZnO lattice, which facilitates efficient charge transport.

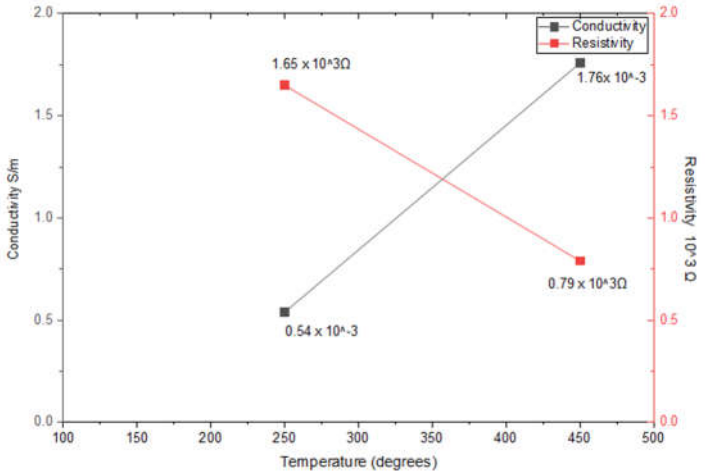

Figure 3.4 Resistivity and Conductivity measured at 250°C (b) at 450°c

4. CONCLUSION

Niobium-doped ZnO thin films synthesized via sol-gel dip coating demonstrated reproducible structural integrity and controlled microstructural evolution. The systematic annealing at 250 °C and 450 °C revealed that thermal treatment plays a decisive role in crystallization behavior, with higher temperatures yielding sharper diffraction peaks, reduced microstrain, and improved lattice ordering. SEM analysis confirmed the presence of uniformly distributed nanoparticles with refined grain morphology, highlighting Nb's effectiveness in stabilizing the ZnO lattice and suppressing abnormal grain growth. These outcomes establish the reliability of the adopted synthesis route and validate Nb doping as a viable strategy for tailoring ZnO thin films.

This study underscores the broader significance of dopant engineering in optimizing functional oxides for advanced applications. By demonstrating that Nb incorporation enhances phase stability, grain refinement, and structural robustness, this work provides a foundation for further exploration of optical and electronic property modulation in ZnO-based systems. The findings position Nb–ZnO thin films as promising candidates for

transparent conducting layers, optoelectronic devices, and energy-related technologies, where controlled crystallinity and defect management are critical to performance.

REFERENCES

1. Kumar, R., et al. (2022). Structural and optical properties of transition metal-doped ZnO thin films prepared by sol-gel method. Journal of Sol-Gel Science and Technology.
2. Singh, P., et al. (2023). Microstructural evolution in doped ZnO thin films synthesized via dip coating. Ceramics International.
3. Li, Y., et al. (2023). Effect of niobium doping on ZnO thin films for transparent conducting applications. Applied Surface Science.
4. Jafarov, M. A., Nasirov, E. F., & Jahangirova, S. A. (2025). Sol–gel synthesis of zinc oxide thin films. Semiconductors, 59, 369–373.
5. Eswar, K. A., Rostan, N. F., Mohamad, M., Md Akhir, R., & Rosfaya, R. (2025). Effect of niobium dopant on ZnO thin films prepared via the sol–gel spin coating method. Science Journal, Universitas Indonesia, 29(1).
6. Solaymani, S., Sabbaghzadeh, J., Kulesza, S., Bramowicz, M., Ghaderi, A., Tajbakhsh, N., Dejam, L., Mohammadpour, M., Ţălu, Ş., Rychlik, K., & Salehi Shayegan, A. (2025). Exploring the morphological and optical properties of N-doped ZnO heterojunctions. Journal of Materials Science: Materials in Electronics, 36, 115.
7. Khan, M., Nowsherwan, G. A., Ali, R., Ahmed, M., Anwar, N., Riaz, S., Farooq, A., Hussain, S. S., Naseem, S., & Choi, J. R. (2023). Investigation of photoluminescence and optoelectronic properties of transition metal-doped ZnO thin films. Molecules, 28(24).
8. Kamalianfar, A. (2025). Optical band gap engineering and comparison of conductivity of Nb- and Ta-doped ZnO thin films. Journal of Engineering and Applied Research, 2(2), 49–63.
9. Zohora Toma, F. T., Rahman, M. S., & Maria, K. H. (2025). A review of recent advances in ZnO nanostructured thin films by various deposition techniques. Discover Materials, 5, 60.
10. Rakesh, K., et al. (2023). Electrochemical synthesis and characterization of Nb-doped ZnO nanoparticles. Journal of Materials Science.

11. Pawar, S. M., et al. (2022). Effect of dopant incorporation on ZnO thin films prepared by sol-gel method. Materials Chemistry and Physics.
12. Singh, P., et al. (2021). Review on ZnO thin films: Doping strategies and property modulation. Thin Solid Films.
13. Gokulakrishnan, V., Parthiban, S., Jeganathan, K., & Ramamurthi, K. (2011). Structural, optical, and electrical properties of Nb-doped ZnO thin films prepared by spray pyrolysis method. Journal of Electronic Materials, 40(12), 2382–2387.
14. Lovchinov, K., Angelov, O., & Dimova-Malinovska, D. (2012). Electrical and optical properties of ZnO thin films doped with Nb deposited by RF magnetron sputtering. Journal of Physics: Conference Series, 356, 012026.
15. Xu, J. W., Wang, H., Jiang, M. H., & Liu, X. Y. (2010). Properties of Nb-doped ZnO transparent conductive thin films deposited by RF magnetron sputtering. Bulletin of Materials Science, 33(2), 119–122.